Paleoproductivity during the middle Miocene carbon isotope events: A data-model approach

Liselotte Diester-Haass,[1] Katharina Billups,[2] Ingrid Jacquemin,[3] Kay C. Emeis,[4] Vincent Lefebvre,[5] and Louis François[3]

[1]   To what extent are individual middle Miocene eccentricity-scale benthic foraminiferal carbon isotope maxima (the so-called CM events) related to changes in marine export productivity? Here we use benthic foraminiferal accumulation rates from three sites in the Pacific and Southern Oceans and a geochemical box model to assess relationships between benthic foraminiferal $\delta^{13}C$ records, export productivity, and the global carbon cycle. Results from Deep Sea Drilling Project Hole 588 and Ocean Drilling Program Site 747 show a distinct productivity maximum during CM 6 at 13.8 Ma, the time of major expansion of ice on Antarctica. Productivity maxima during other CM events are only recorded at high-latitude Site 747. A set of numerical experiments tests whether changes in foraminiferal $\delta^{13}C$ records (CM events) and export productivity can be simulated solely by sea level fluctuations and the associated changes in global weathering-deposition cycles, by sea level fluctuations plus global climatic cooling, and by sea level fluctuations plus invigorated ocean circulation. Consistent with data, the periodic forcing of sea level and albedo (and associated weathering cycles) produces $\delta^{13}C$ variations of the correct temporal spacing, albeit with a reduced amplitude. A productivity response of the correct magnitude is achieved by enhancing ocean circulation during cold periods. We suggest that the pacing of middle Miocene $\delta^{13}C$ fluctuations is associated with cyclical sea level variations. The amplitude, however, is muted perhaps due to the competing effects of a time-lagged response to sea level lowstands but an immediate response to invigorated ocean circulation during cold phases.

1.   Introduction

[2] Carbon isotope excursions in the marine carbonate (e.g., foraminiferal) record provide an opportunity to study past perturbations of the carbon cycle [e.g., *Zachos et al.*, 2001; *Veizer et al.*, 1999; *Kump and Arthur*, 1999; *Zachos and Kump*, 2005]. Because reduced carbon in organic matter is depleted in ^{13}C relative to oxidized carbon in carbonates,

large variations in the $\delta^{13}C$ values of marine carbonate reflect changes in the fraction of organic matter burial in sediments [e.g., *Vincent and Berger*, 1985; *Kump and Arthur*, 1999; *Zachos et al.*, 2001]. The importance of increased burial of organic matter in sediments with respect to understanding climate change lies in their potential association with increased surface water primary productivity (the other being enhanced preservation), and hence a potential means to remove CO_2 from the ocean-atmosphere system. A case in point is the $\delta^{13}C$ maximum characterizing the Eocene-Oligocene boundary [*Zachos and Kump*, 2005] and the $\delta^{13}C$ maximum across the Oligocene-Miocene climate transition [*Pälike et al.*, 2006], both having been explained by enhanced primary productivity and carbon burial during periods of Antarctic ice sheet expansion [*Diester-Haass and Zahn*, 1996; *Zachos and Kump*, 2005; *Diester-Haass et al.*, 2011].

[3] One well-studied interval of time characterized by a long-lasting, positive carbon isotope excursion occurs during the early through middle Miocene (~13–18 Ma). Enhanced organic matter burial in the circum Pacific margin, the so-called "Monterey Event" [*Vincent and Berger*, 1985], has been called upon to explain the overall $\delta^{13}C$ maximum. However, organic matter accumulation rates at the California margin of the eastern Pacific are too low to be

responsible for the global positive $\delta^{13}C$ excursion [*Isaacs*, 2001; *Föllmi et al.*, 2005]. Furthermore, there is no evidence for enhanced organic carbon burial in marine sediments, and a geochemical box model experiment suggests that marine productivity changes are unlikely to be a cause of the overall benthic foraminiferal $\delta^{13}C$ maximum between 18 and 13 Ma [*Diester-Haass et al.*, 2009]. To explain the long-term carbon isotope excursion, carbon storage on land such as in widespread coal deposits is the most likely explanation [*Utescher et al.*, 2000; *Föllmi et al.*, 2005; *Holdgate et al.*, 2007].

[4] Superimposed on this long-term excursion, benthic foraminiferal carbon isotope records display a series of shorter-term positive excursions (the so-called CM events after *Woodruff and Savin* [1991]). These CM events are associated with increases in foraminiferal $\delta^{18}O$ values suggesting a tangible link with intervals of glaciations [*Flower and Kennett*, 1993]. Orbital tuning of high-resolution stable isotope records also links each individual CM event with the long-term component of eccentricity (~400 kyr) [*Holbourn et al.*, 2007]. For the Oligocene-Miocene boundary, where carbon and oxygen isotope records also covary, the inference that the link is one via marine export production coupled to organic matter burial is backed by a geochemical model [*Pälike et al.*, 2006]. Also, the link has since then been supported by proxy reconstructions of export paleoproductivity, which distinctly increases at the Oligocene-Miocene boundary as well as during the 400 kyr paced $\delta^{13}C$ maxima spanning this interval of time [*Diester-Haass et al.*, 2011]. For the Miocene, the positive relationship between carbon and oxygen isotope records at the eccentricity scale was also inferred to reflect changes in the global carbon cycle via marine productivity and organic matter burial [*Holbourn et al.*, 2007], although up to now, neither proxy evidence nor geochemical modeling output exists in support of this.

[5] In this study we examine whether or not individual middle Miocene CM events can be linked to changes in marine export productivity in a manner akin to the processes important during the Eocene to Oligocene and the Oligocene to Miocene climate transitions. As in a previous study of the Oligocene/Miocene boundary interval [*Diester-Haass et al.*, 2011], we use benthic foraminiferal accumulation rates (BFARs) as a proxy for export production [*Herguera*, 2000]. Export production reflects the amount of organic matter settling from the photic zone and thus the pathway of CO_2 out of the surface ocean-atmosphere system. We follow up on the proxy reconstructions with a geochemical box model to simulate aspects of the carbon cycle. Specifically, we test whether CM events reflect (1) nutrient input variability via sea level fluctuations and the associated changes in global weathering-deposition cycles, (2) global climatic cooling, and (3) ocean circulation patterns.

2. Methods

2.1. Site Selection

[6] We reconstructed BFARs at three sites. Two sites are located in the southern Pacific Ocean (Deep Sea Drilling Project (DSDP) Hole 588A, and Ocean Drilling Program (ODP) Site 1171), and one lies in the Indian Ocean sector of the Southern Ocean (ODP Site 747); they represent a meridional transect of hydrographic regimes ranging from

the subtropical gyre to the south of the modern ocean Polar Frontal Zone (Figure 1). Together with published data from the Atlantic Ocean (ODP Sites 925 and 1265 and DSDP Site 608, see Figure 1 for location) [*Diester-Haass et al.*, 2009], the data set allows us to investigate the extent to which individual Miocene CM events are indeed related to global ocean processes.

2.1.1. DSDP Hole 588A

[7] DSDP Hole 588A was drilled in 1533 m water depth on the Lord Howe Rise in the southwestern subtropical Pacific (26°S, 161°E; Figure 1 and Table 1). During the Neogene the site has moved by about 5° from 31°S to the present latitude [*Kennett and von der Borch*, 1986] and may have been located within the high-productivity zone of the subtropical divergence that is today at 30°S [*Elmstrom and Kennett*, 1986]). In the modern ocean, Hole 588A underlies the waters of the western boundary current of the south Pacific subtropical gyre. As is typical for western boundary currents, present-day primary productivity is relatively low ranging from 10 to 15 g C cm^{-2} kyr^{-1} [*Antoine et al.*, 1996].

[8] Our age model for Hole 588A is based on *Holbourn et al.* [2007], who correlated published $\delta^{18}O$ record to that of orbitally tuned Sites 1146 and 1237. Accordingly, 12 depth-age control points assign ages from 12.4 to 15.3 Ma to the upper 62 m of the studied section. For the older portion of the record (308–333 m below seafloor (mbsf)), we use the Hole 588A benthic foraminiferal $\delta^{13}C$ record generated here to align three $\delta^{13}C$ maxima between 15.5 and 17 Ma with CM 3b (15.75 Ma), CM 3a (16.15 Ma), and CM 2 (16.5 Ma); ages of CM events are from *Holbourn et al.* [2007]. As we show below, excellent agreement between the timing of the older $\delta^{13}C$ maxima at Hole 588A and the published ages of the older CM events can be achieved in this manner (Table 2). Given sedimentation rates of at least 1 cm kyr^{-1}, we sampled the section from 245.8 to 333.6 mbsf at about 50 cm spacing to yield a sample resolution of approximately 60 kyr, which is sufficiently high to resolve potential productivity variations related to 400 kyr paced CM events.

2.1.2. ODP Site 1171

[9] ODP Leg 189 Site 1171 was drilled on the South Tasman Rise in 2150 m water depth (48°30′S, 149°06.69′E; Figure 1 and Table 1). The South Tasman Rise has moved from a location at 58°S at 20 Ma, to 55°S at 14 Ma, and to the present position at 48°S [*Lawver et al.*, 1992; *Ennyu and Arthur*, 2004]. Paleodepth increased from 1600 to 2150 m [*Hill and Exon*, 2004]. Because of the northward migration of the South Tasman Rise, the hydrography and surface water temperatures likely changed significantly since the Miocene [*Nelson and Cooke*, 2001; *Ennyu and Arthur*, 2004]. In this area, very strong surface and bottom currents are associated with the Antarctic Circumpolar Current. Present-day productivity is relatively low (5–10 g C cm^{-2} kyr^{-1}, *Antoine et al.*, 1996).

[10] Site 1171 from the South Tasman Rise has also been dated by *Holbourn et al.* [2007]. They orbitally tuned the published stable isotope record from Site 1171 and derived 16 age control points between 12.8 and 16.1 Ma (Table 2). Our productivity record ends at 17.0 Ma, and we extrapolate ages below 16.1 Ma assuming constant linear sedimentation rates. Given sedimentation rates of on average 1–2 cm kyr^{-1}, we sampled the section from 129 to 217 mbsf at 60–70 cm
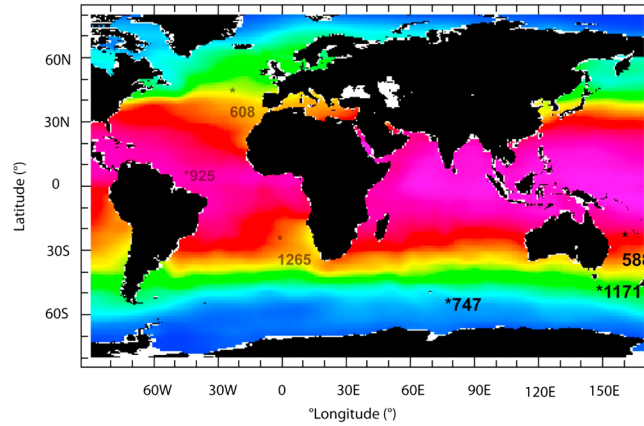
Figure 1. Location of sites investigated in this study (see also Table 1). Colors reflect annual average sea surface temperatures [*Levitus and Boyer*, 1994]. The figure was generated using the interactive website of the Lamont Doherty Geological Observatory.

intervals to obtain a spacing of on average 40 kyr, which is sufficient to resolve eccentricity-scale (~400 kyr) variations in paleoproductivity.

2.1.3. ODP Site 747

[11] Site 747 is located on the Kerguelen Plateau in the Southern Indian Ocean at 54°48.68′S, 76°47.64′E in 1697 m water depth (Figure 1 and Table 1). The paleodepth cannot be estimated by backtracking [*Schlich et al.*, 1989]. Today the site is located 500 km south of the polar front (Antarctic convergence). Changes in surface water productivity, aside from seasonal changes in light levels that dominate productivity in the modern ocean, are attributed to upwelling on the eastern side of the plateau [*Mackensen and Ehrmann*, 1992]. Present-day productivity at Site 747 is 5–10 g C cm^{-2} kyr^{-1} [*Antoine et al.*, 1996].

[12] We use the age model published by *Majewski and Bohaty* [2010], which is based on diatom biostratigraphy and magnetostratigraphy with ages reported on the *Lourens et al.* [2004] timescale. We linearly interpolate between age control points. To resolve productivity variations associated with individual CM events, we sampled the section from 50.3 to 106.90 mbsf at 20–40 cm intervals. At average sedimentation rates of about 0.6 cm kyr^{-1}, this sampling scheme results in an about 60 kyr time step for individual data points. As we shall show below, the comparatively high-resolution δ^{13}C record generated here illustrates excellent agreement between the timing of δ^{13}C maxima and the CM events in support of this age model (Table 2).

2.2. Benthic Foraminiferal Accumulation Rates and Paleoproductivity

[13] Accumulation rates (ARs) are commonly used to assess temporal changes in the accumulation of individual sediment components such as CaCO$_3$, SiO$_2$, or benthic foraminifera. Accumulation rates are necessary in order to account for relative changes in one sediment component versus another (a "closed sum" problem). To calculate ARs, we first linearly interpolate between age control points to derive linear sedimentation rates (LSRs, cm kyr^{-1}). LSRs are then multiplied by the shipboard dry bulk densities (g cm^{-3}) (Hole 588A: *Kennett and von der Borch* [1986]; Site 1171: *Shipboard Scientific Party* [2001]; Site 747: *Schlich et al.* [1989]). Benthic foraminiferal accumulation rates (BFARs) are derived by multiplying the number of tests per gram sediment (noBF) with the AR and are expressed as cm^{-2} kyr^{-1}.

[14] Accumulation rates of benthic foraminiferal tests on the seafloor have been used extensively as a proxy for paleoproductivity [*Herguera and Berger*, 1991; *Nees*, 1997; *Schmiedl and Mackensen*, 1997; *Yasuda*, 1997; *van der Zwaan et al.*, 1999; *Diester-Haass et al.*, 2004, 2005, 2006; *Diester-Haass and Nees*, 2004; *Holbourn et al.*, 2005; *Waite et al.*, 2008]. The proxy is based on a quantitative relationship between primary productivity and the organic carbon flux reaching the seafloor [*Berger and Wefer*, 1990] and benthic foraminiferal accumulation rates calibrated using core top sediments from the Atlantic and Pacific Oceans [*Herguera*, 2000]. The organic carbon flux parameter accounts for the

Table 1. Summary of Site Locations and Settings

Location	Water Depth (m)	Latitude/Longitude	Productivity[a] (g C cm^{-2} kyr^{-1})	Sediment Type
DSDP 94 Hole 588A[b]	1533	26°S/161°E	10–15	nannofossil ooze
ODP 189 Site 1171C[c]	2150[d]	55°S/149°E[e]	5–10	chalk and ooze
ODP 120 Site 747A[f]	1697	54°S/77°E	5–10	nannofossil ooze

[a]*Antoine et al.* [1996].
[b]*Kennett and von der Borch* [1986].
[c]*Shipboard Scientific Party* [2001].
[d]*Hill and Exon* [2004].
[e]*Lawver et al.* [1992] and *Ennyu and Arthur* [2004].
[f]*Schlich et al.* [1989].

Table 2. Comparison of the Timing of Individual Middle Miocene Carbon Isotope Excursions (CM Events)

CM Event	Age (Ma) *Holbourn et al.* [2007]	Age (Ma) Site 588	Age (Ma) Site 1171	Age (Ma) Site 747
6	13.75	13.75	13.75	13.75
5b	14.15	14.07	14.09	14.30
5a	14.55	14.54	14.61	
4b	14.95	15.01	[a]	14.93
4a	15.35	15.33	15.33	15.40
3b	15.75	15.78	15.78	15.75
3a	16.15	16.15	16.08	16.11
2	16.50	16.46	[a]	16.47
1	16.90	16.89	[a]	16.91

[a]No δ^{13}C maxima corresponding to these events.

degree of degradation in the water column (as a function of water depth, which is quantitatively much more significant than the subsequent degradation at the seafloor; *Suess* [1980]). Thus, BFARs themselves reflect export production and further carbon degradation through the water column. As illustrated by *Herguera* [2000], a link to (paleo) primary productivity (in g C cm^{-2} kyr^{-1}) at the sea surface can be made:

$$PP = 0.4Z \times BFAR^{0.5} \qquad (1)$$

where PP stands for paleoproductivity and is related to the flux of organic carbon to the seafloor (g C cm^{-2} kyr^{-1}), Z is the water depth, and BFAR is the benthic foraminifer accumulation rate (number cm^{-2} kyr^{-1}), which is calculated by multiplying the counted foraminifer tests per gram of sediment with the MARs.

[15] There are several uncertainties and limitations to this method. Foremost, age control affects this parameter via linear sedimentation rates needed to calculate ARs. Short-term changes in sedimentation and accumulation rates are thus masked. In order to rule out that linear sedimentation rates drive the BFARs, we compare the thus-derived results with the original number of tests/gram sediment sample. Because the number of benthic foraminifera of a sample can be influenced by carbonate dissolution, we also monitor dissolution using the ratio of benthic to planktic foraminifera as well as counting the percent fragments in each sample. The link with surface water productivity assumes that the degree of organic matter degradation in the water column remains constant through time and that the paleowater depth can be determined. These factors preclude any quantitative comparison to modern-day productivity, but it allows an estimate of the relative magnitude of the variations at any point in time on the same scale of modern-day productivity. Despite these uncertainties, meaningful export paleoproductivity estimates can be obtained in this manner as illustrated, for example, by the covariance of paleoproductivity with the benthic foraminiferal δ^{13}C record across the Oligocene/Miocene boundary [*Diester-Haass et al.*, 2011].

2.3. Analytical Methods

[16] Samples (20 cm^3) were split for geochemical and micropaleontological analyses. Subsamples of 10 cm^3 were oven-dried at 60°C, weighed, washed through a 63 μm sieve, dried, and dry-sieved into subfractions (63–150, 150–250, 250–500, >500 μm) for sedimentological-micropaleontological

studies. In each fraction, 800 grains (if present) were counted, and various biogenic, clastic, and authigenic components were differentiated to yield the percentage composition of the sand fraction. The numbers of benthic foraminifera in the fractions >150 μm were summed up and divided by the weight of the total analyzed sample to give the number of benthic foraminifera per gram of total sediment.

[17] Stable isotope analyses were conducted on 1–5 *Cibicidoides wuellerstorfi* and *Cibicidoides mundulus* picked from the >255 μm fraction. All samples were sonicated in de-ionized water to remove adhering sediment and oven-dried for at least 24 h prior to isotope analysis. Analyses were performed at the University of Delaware using a GVI IsoPrime instrument equipped with a MultiPrep periphery for the automated reaction of individual samples with phosphoric acid (at 90°C). Based on repeated measurements of NBS-19 and an in-house standard (Carrara Marble), the precision for δ^{13}C and δ^{18}O values is better than 0.05‰ and 0.08‰, respectively, in the calcium carbonate mass range of the samples (20–200 μg).

2.4. Geochemical Box Model

[18] To assess potential relationships between the benthic foraminiferal-derived productivity and the CM events, we use an updated version of the box model used by *Diester-Haass et al.* [2009] and further developed by *Lefebvre* [2009] and *Lefebvre et al.* [2010]. This carbon cycle box model is coupled to an energy balance climate model [*François and Walker*, 1992] and, in the version used here, contains four reservoirs for the global ocean (low-latitude surface ocean, low-latitude thermocline, high-latitude surface ocean, deep ocean) and one for the atmosphere. It calculates the budgets of carbon, alkalinity, phosphorus, and dissolved oxygen in the ocean reservoirs and those of carbon dioxide (CO_2) and oxygen (O_2) in the atmosphere. The carbon isotope budget (δ^{13}C values of dissolved inorganic carbon) is also calculated for each reservoir, as well as carbonate speciation. Biological productivity in the surface ocean reservoirs is driven by phosphorus inputs to these reservoirs. This model productivity reflects export production (i.e., the productivity related to the amount of organic matter escaping oxidation in the surface reservoirs and transferred to the thermocline or to the deep ocean reservoir) and thus corresponds to the BFAR-derived productivity data.

[19] The model is similar in its conception to the carbon cycle model developed by *Walker and Kasting* [1992] and used by *Pälike et al.* [2006] to study Oligocene eccentricity cycles. However, it includes a more detailed treatment of weathering with weathering rates calculated in every 10° latitude band (the resolution of the climate model) for four types of rocks (basalts, other silicate rocks, carbonates, and organic-rich sedimentary rocks). Weathering rate laws are based on field data [*Gaillardet et al.*, 1999; *Millot et al.*, 2002; *Dessert et al.*, 2001, 2003]. Additional feedbacks are also incorporated in the model via the inclusion of an oxygen cycle and the variation of the carbon:phosphorus ratio of buried organic matter in concert with the oxygenation level of the ocean [*Van Cappellen and Ingall*, 1996].

[20] Compared to the model used by *Pälike et al.* [2006], our model has both more sophisticated carbon cycle and
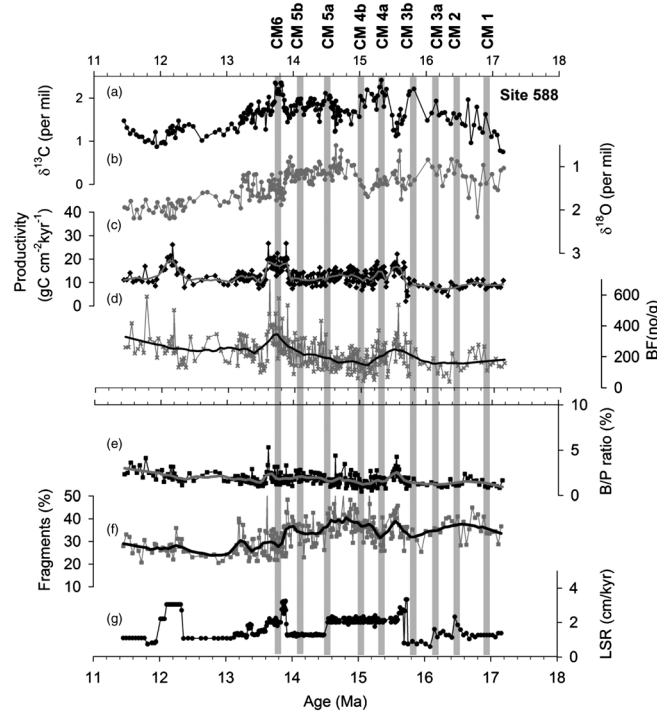
Figure 2. Results from southwestern subtropical Pacific Site 588. (a) Benthic foraminiferal $\delta^{13}C$ values, (b) benthic foraminiferal $\delta^{18}O$ values, (c) benthic foraminiferal mass accumulation rate-derived export paleoproductivity, (d) number of benthic foraminiferal tests per gram sediment, (e) percent benthic to planktonic (B/P) foraminiferal test ratio, (f) percent fragments, and (g) linear sedimentation rates (LSRs). Vertical grey bars highlight the position of Miocene carbon-isotope (CM) events after *Holbourn et al.* [2007]. Heavy lines in Figures 2c–2f reflect a Gaussian smoothing function with a 3% sampling portion.

climate modules, but lacks an ice sheet module. Therefore, we use sea level fluctuations as inputs to our model (see section 5). Sea level changes modify the land and shelf areas, as well as the volumes of the ocean reservoirs. They thus impact weathering, as well as carbonate and organic carbon seawater concentrations and burial. A short description of the model can be found in the supporting information.

3. Results

3.1. Site 588

[21] Hole 588 has been instrumental in reconstructing Miocene subtropical Pacific paleoceanography, and individual CM events are easily identified [*Flower and Kennett*, 1993, 1994]. In order to directly compare the marine export productivity derived from benthic foraminifers with the $\delta^{13}C$ records, we have generated stable isotope data from the same samples for which BFARs were calculated (Figure 2a). Hole 588A benthic foraminifer $\delta^{13}C$ values exhibit the well-known positive carbon isotope excursion beginning at ~17 Ma and ending at ~13 Ma with a return to preexcursion values (Figure 2a). Superimposed on the long-term trend are several well-defined $\delta^{13}C$ maxima, the so-called CM events (Figure 2a and Table 2) [*Flower and Kennett*, 1994; *Holbourn et al.*, 2007]. Over the long term, the positive $\delta^{13}C$ excursion corresponds to an interval of relatively low $\delta^{18}O$ values, but individual $\delta^{18}O$ maxima accompany the CM events in $\delta^{13}C$ and point to a relationship between cooling events and the deep oceanic carbon reservoir [*Flower and Kennett*, 1994]. The $\delta^{18}O$ values

increase rapidly at 13.9 Ma and mark the major step in mid-Miocene cooling and Antarctic ice sheet development (Figure 2b). This increase in $\delta^{18}O$ is coincident with the $\delta^{13}C$ increase that leads to the most pronounced of the CM events, CM 6.

[22] At Hole 588A, there is no consistent association between BFAR-derived export productivity and the $\delta^{13}C$ record on either the longer term or on the scale of individual CM events (Figure 2c). Relatively constant export paleoproductivity values that are close to modern ocean values are punctuated by three distinct maxima at 15.5 Ma (between CM 3b and CM 4a), at 13.8 Ma (CM 6), and at 12.2 Ma. At this site, CM 6 is thus the only CM event that is accompanied by an increase in export productivity. The maximum at CM 6 (as well as the older one at 15.5 Ma) is not an artifact of increased sedimentation rates at this time because it is apparent in the concurrently high number of benthic foraminiferal tests per gram sediment (Figure 2d). The shape of the maximum, however, in particular the abrupt increase at 13.9 Ma, may be linked to the similarly abrupt increase in sedimentation rates (Figure 2g). That the benthic foraminiferal maximum during CM 6 is not due to the enhanced dissolution of other carbonate phases is apparent in the relatively constant benthic to planktonic (B/P) ratio (Figure 2e) as well as a decrease in the percent fragments (Figure 2f) at this time.

3.2. Site 1171

[23] High-resolution benthic foraminifer stable isotope records for the site are discussed by *Shevenell and Kennett*
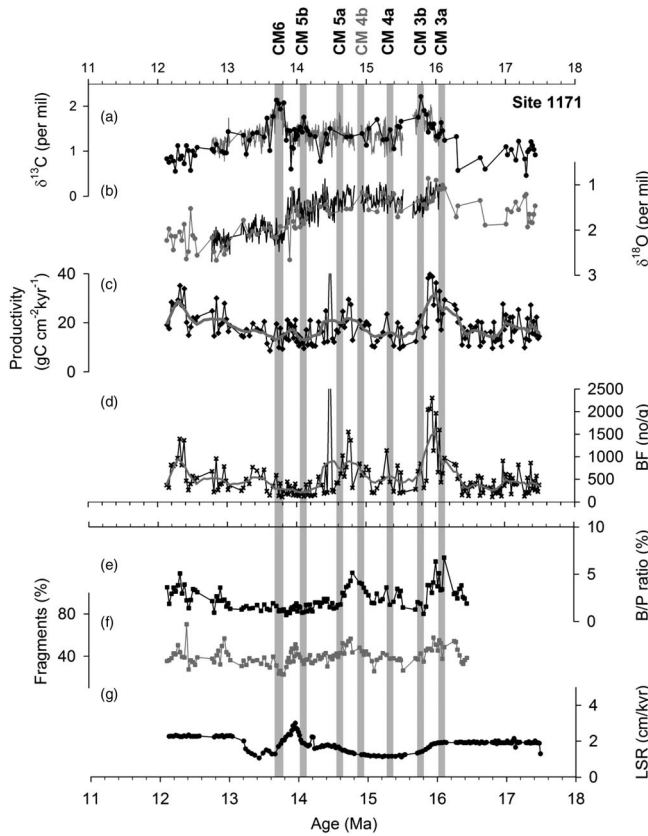
Figure 3. Results from southwestern Pacific Site 1171. (a) Benthic foraminiferal δ^{13}C values, (b) benthic foraminiferal δ^{18}O values, (c) benthic foraminiferal mass accumulation rate-derived export paleoproductivity, (d) number of benthic foraminiferal tests per gram sediment, (e) percent benthic to planktonic (B/P) foraminiferal test ratio, (f) percent fragments, and (g) linear sedimentation rates (LSR). Vertical grey bars highlight the position of Miocene carbon-isotope (CM) events after *Holbourn et al.* [2007]). Heavy line in Figures 2c and 2d reflects a Gaussian smoothing function with a 3% sampling portion.

[2007] and *Shevenell et al.* [2008], and we generated only new data of relatively low resolution in this study (Figures 3a and 3b). The benthic foraminiferal δ^{13}C record shows a long-term positive middle Miocene excursion beginning with an increase in values between 16.4 and 16 Ma and ending after a well-pronounced and prolonged maximum centered on 13.75 Ma (CM 6) (Figure 3a). Smaller-scale CM events are apparent in the record, and maxima in δ^{13}C correspond to CM events at 16.1 Ma (CM 3a), 15.8 Ma (CM 3b), 15.33 Ma (CM 4a), 14.61 Ma (CM 5a), 14.07 Ma (CM 5b), and 13.8 Ma (CM 6) (Table 2). Although CM 6 and CM 5b are associated with δ^{18}O maxima, other individual CM events lack distinct δ^{18}O maxima (Figures 3a and 3b).

[24] As at Site 588, there is no equivalent long-term pattern in export productivity (indicated by benthic foraminifers) to parallel the entire mid-Miocene δ^{13}C shift, and productivity and δ^{13}C values do not show a consistent relationship on shorter timescales (Figure 3c). A pronounced productivity maximum at 15.9 Ma is outlined during a δ^{13}C minimum

between CM 3a (16.1 Ma) and CM 3b (15.8 Ma). Other pronounced productivity maxima occur at 14.9 Ma (CM 4b), 14.7 Ma (between CM 4b and CM 5a), and 13.9 Ma (between CM 5b and CM 6). The δ^{13}C maximum of CM 6 (13.8 Ma) is not associated with a matching maximum in export productivity. The high number of benthic foraminiferal tests supports only the older productivity maxima, so that the maximum at 13.8 Ma may be an artifact of high LSR at this time (Figure 3g). For scale, minimum paleoproductivity of 10–20 g C cm^{-2} kyr^{-1} at this site is higher than modern-day values (5–10 g C cm^{-2} kyr^{-1}), which may, however, reflect uncertainties in the paleobathymetry or change in paleohydrographic conditions.

3.3. Site 747

[25] Site 747 has also been studied extensively to reconstruct Miocene paleoceanography, and CM events are clearly expressed in its stable isotope record [*Wright and Miller*, 1992; *Verducci et al.*, 2009]. *Cibicidoides* are abundant in the sampled sediment volume, and we were able to construct continuous records to correspond directly to the export productivity proxy. The broad middle Miocene positive δ^{13}C excursion is delineated by increasing values between
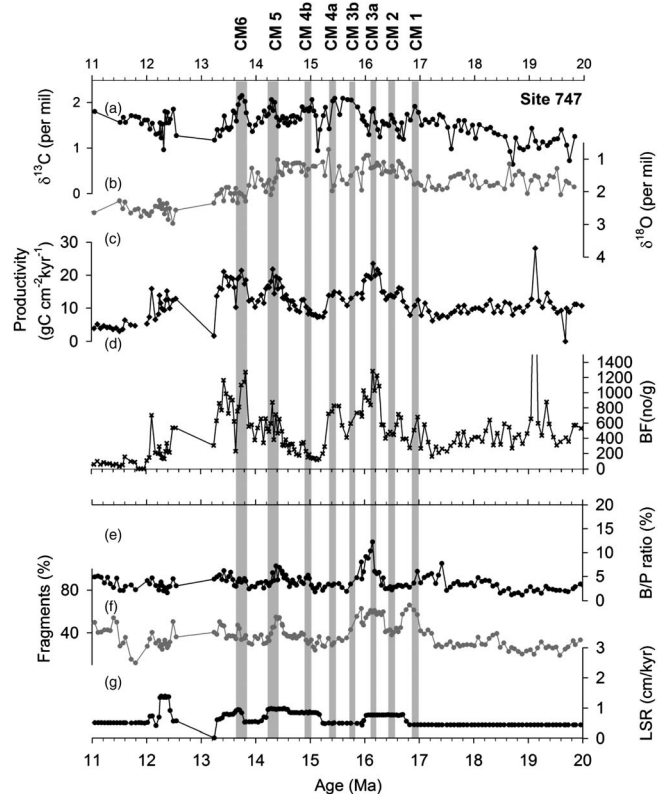

Figure 4. Results from Southern Ocean Site 747. (a) Benthic foraminiferal δ^{13}C values, (b) benthic foraminiferal δ^{18}O values, (c) benthic foraminiferal mass accumulation rate-derived export paleoproductivity, (d) number of benthic foraminiferal tests per gram sediment, (e) percent benthic to planktonic (B/P) foraminiferal test ratio, (f) percent fragments, and (g) linear sedimentation rates (LSR). Vertical grey bars highlight the position of Miocene carbon-isotope (CM) events after *Holbourn et al.* [2007].
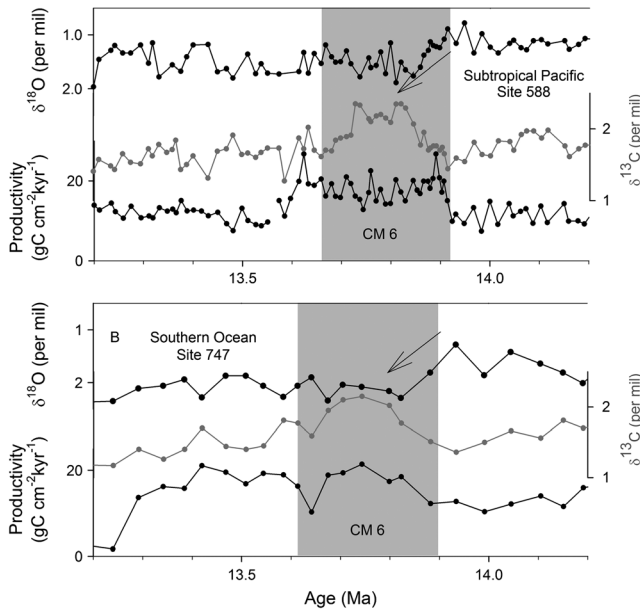
Figure 5. Comparison of $\delta^{13}C$, $\delta^{18}O$ and export paleoproductivity records focused on CM 6 at Site 588 (A) and 747 (B). Benthic foraminiferal $\delta^{13}C$ values, benthic foraminiferal $\delta^{18}O$ values, export paleoproductivity in gC/cm^2 x ky derived from benthic foraminiferal mass accumulation rates.

17 and 16 Ma and decreasing values after 13.5 Ma with the end of CM 6 (Figure 4a). Shorter-term $\delta^{13}C$ variations superimposed on the long-term plateau are closely related to the CM events, as well as to maxima in the $\delta^{18}O$ record [e.g., *Wright and Miller*, 1992; *Wright et al.*, 1992] (Figures 4a and 4b). There is excellent agreement between the $\delta^{13}C$ maximum at 13.75 Ma and the age of CM 6. The timing of other individual $\delta^{13}C$ maxima corresponds to published ages of CM 5–CM 1 (Table 2).

[26] As at the other sites, the long-term trend in export paleoproductivity does not parallel the positive $\delta^{13}C$ maximum, but at this site, a number of individual productivity maxima occur consistently during the majority of the CM events (CM 1, CM 3a, CM 4a, CM 5, and CM 6; Figure 4c). All of these productivity maxima are supported by maxima in the abundance of benthic foraminiferal tests (Figure 4d) and are thus not primarily driven by variations in sedimentation rates (Figure 4g). However, we point out that in the majority of the cases the productivity maxima are broader than the $\delta^{13}C$ maxima. During CM 6, however, paleoproductivity values do increase concurrently with $\delta^{13}C$ and $\delta^{18}O$ values. For CM 6, paleoproductivity remains high after benthic foraminifer $\delta^{13}C$ values have returned to low values, creating a prolonged double peak. The productivity maxima of CM 5, CM 3a, and CM 1 are accompanied by increases in the B/P ratio and the percent fragments in the sediments (Figures 4e and 4f, respectively) and may in part be related to enhanced dissolution. However, this is not the case for CM 6 when both indices remain constant. For scale, minimum paleoproductivity at this site remains close to modern-day values (5–10 g C cm^{-2} kyr^{-1}), with a factor of 2 increase during CM 6. Although comparison of absolute productivity values is limited by uncertainties in the paleobathymetry, the increase during CM 6 is robust.

4. Interim Synthesis

[27] During the middle Miocene $\delta^{13}C$ maximum, the Monterey Event, none of the Pacific Ocean sites investigated here experienced a long-term response in marine export productivity. These results agree with the observations of *Diester-Haass et al.* [2009] who found no evidence for long-term changes in productivity to parallel Atlantic Ocean benthic foraminiferal $\delta^{13}C$ records during this interval of time.

[28] As evidenced by the Pacific records presented here, individual CM events are not consistently associated with paleoproductivity maxima. CM 6 is recorded distinctly as an increase in export paleoproductivity only at subtropical Site 588 as well as Southern Ocean Site 747. At these two sites, however, increases in paleoproductivity parallel increases in $\delta^{13}C$ during the CM 6 event (Figures 5a and 5b, respectively), suggesting a coupling between the records. At Site 747, most of the other CM events also occur with enhanced productivity, but the duration of the events is not the same. These results lead us to conclude that the middle Miocene $\delta^{13}C$ events, although of similar amplitude and temporal variability as their Eocene/Oligocene and Oligocene/Miocene counterparts, may not be directly related to global paleoproductivity.

[29] We recognize that on the scale of individual CM events, our results are ambiguous because productivity and $\delta^{13}C$ variations are not consistently coupled at all sites. Whether or not this is due to the role of external factors driving $\delta^{13}C$ records and productivity such as nutrient input related to weathering on land, or internal factors such as enhanced nutrient uptake due to changes in ocean circulation, or perhaps a combination of both, can be examined using geochemical box models.

[30] Specifically, we ask what factors exhibiting variability over the 400 kyr eccentricity cycle that appears to pace the CM events [*Holbourn et al.*, 2007] may have impacts on the ocean carbon cycle and the carbon isotope budget. For instance, what is the potential contribution of sea level change on the ^{13}C budget of the deep ocean? Rising or lowering sea level alters the fluxes of continental weathering, carbonate deposition, and organic carbon deposition, since the continental and shelf areas are modified. Eccentricity-driven climatic fluctuations, through surface temperature and continental runoff changes, can also be expected to impact weathering and carbon deposition processes and hence the carbon isotope budget. On the other hand, ocean circulation changes driven by climatic cycles can also affect the carbon cycle via the enhanced delivery of nutrients to the surface ocean stimulating primary productivity and subsequent burial in sediments. What are the relative contributions of these various factors to the isotopic budget of the deep ocean? In the next section, we attempt to evaluate these contributions quantitatively by using an extended version of the global ocean carbon cycle box model described above (see also the supporting information).

5. Numerical Sensitivity Experiments

[31] A set of simulations of the carbon cycle is performed to test whether changes in export productivity and CM events can be caused (1) solely by sea level fluctuations and the
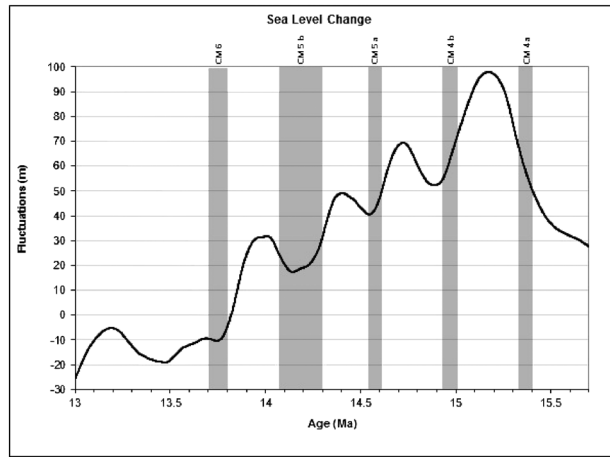
Figure 6. Variation of sea level used in the model simulations. These sea level data are derived from $\delta^{18}O$ values from *Holbourn et al.* [2007] assuming a linear relationship between both variables, an increase of 0.1‰ in $\delta^{18}O$ corresponding to a drop of 10 m in sea level. The timing of CM events (Table 2) is indicated by the vertical shading. The width of the shading is to account for age model uncertainties in the timing of the CM events in our data. See Table 2 for more precise ages of CM events from *Holbourn et al.* [2007].

associated changes in global weathering-deposition cycles, or (2) by global climatic cooling in addition to sea level changes, or else (3) by sea level changes plus invigorated ocean circulation patterns. To this end, we only vary sea level in run 1 to induce changes in weathering. Then we add albedo forcing in run 2 to simulate effects of climate change, and finally we combine the effect of variations in ocean circulation with sea level changes (run 3). The main features of the model are outlined in supporting information.

5.1. Sensitivity to Sea Level and Weathering (Run 1)

[32] In this first simulation, the carbon cycle model is forced with the sea level fluctuations from *Holbourn et al.* [2007] and Holbourn (personal communication, 2008) (Figure 6). This sea level reconstruction highlights the 400 kyr eccentricity-driven variations, but the higher-frequency fluctuations (40 and 100 kyr; see, e.g., *Shevenell et al.* [2008]) have been filtered. We have chosen to use this reconstruction as forcing in the model, because the resolution of our sedimentary data (productivity, $\delta^{13}C$) does not allow analyzing higher-frequency variations. The reconstruction shows a series of well-marked sea level lowstands corresponding approximately to the times of CM events, except for CM 4b, which occurs 100–200 kyr before the sea level minimum. The curve is extended to the period between 19 and 15.7 Ma, over which the model is run for initialization, but for which the results are not discussed. In the absence of detailed bathymetric data for the Miocene, the model hypsometric curve is derived from the global gridded (5 min resolution) database of present-day land elevation and ocean bathymetry (http://www.ngdc.noaa.gov/mgg/global/etopo5.HTML). When sea level is rising or falling, this hypsometric curve is shifted downward or upward by the corresponding number of meters. This change affects land and shelf areas

in the model, as well as the seafloor areas above the lysoclines or compensation depths in the deep reservoir. The volumes of the oceanic reservoirs are also adjusted, corresponding to some dilution or concentration of the oceanic water. All these changes impact weathering rates on land and deposition rates in the ocean; hence, geochemical and isotopic changes of the oceanic and atmospheric carbon reservoirs can be expected.

[33] The changes in sea level induce changes in land and shelf areas that cause changes in weathering and organic carbon deposition. As seen in Figure 7, however, sea level fluctuations alone are unable to produce significant variations of export productivity: The amplitude of the modeled 400 kyr fluctuations in productivity between 15.7 and 12.7 Ma is very small (Figure 7, solid line). Only the modeled long-term increase between 15 and 13 Ma is significant. This long-term trend is linked to the progressive increase of the land area and, hence, of the input of phosphorus from weathering, accompanying the long-term decrease in sea level. Apparently, this mechanism is inefficient for higher-frequency (400 kyr) oscillations in sea level. The reason is that the amplitudes of the reconstructed 400 kyr sea level fluctuations are smaller than the overall long-term variation between 15 and 13 Ma, implying relatively limited changes in land/shelf areas and thus in the input of phosphorus from weathering in the model at this 400 kyr timescale.

[34] The modeled response of deep ocean $\delta^{13}C$ values, however, is more significant (Figure 8). The model produces a general decrease in $\delta^{13}C$ values between approximately 15 and 12.7 Ma. This long-term trend is associated with the long-term decrease in sea level (Figure 6), as well as the prescribed decrease of organic deposition on land after 14 Ma
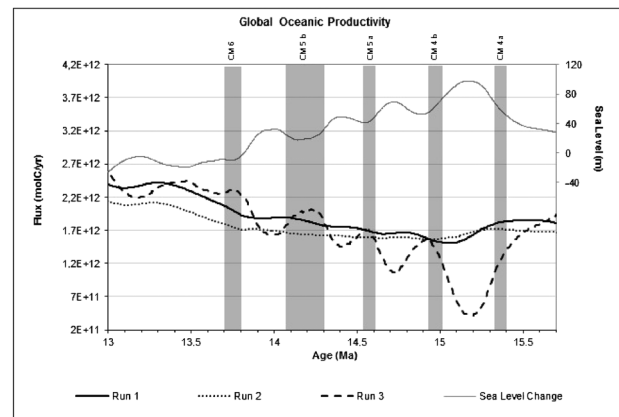

Figure 7. Model variations of global ocean export productivity between 15.7 and 12.7 Ma for three different simulations. Run 1 uses only sea level variations and their impacts on land/shelf areas, ocean hypsometry, and associated changes in weathering. Run 2 corresponds to run 1 simulation with additional high-latitude albedo forcing to produce more significant climate variations, which themselves feedback on weathering rates. Run 3 corresponds to run 1 simulation with varying ocean circulation and associated impacts on ocean productivity (see text). The sea level variation used in the model simulations and the timing of CM events (Table 2) are indicated, respectively, by the grey curve and the vertical shading (Figure 6).

Figure 8. Model variations of deep ocean $\delta^{13}C$ between 15.7 and 12.7 Ma for three different simulations. The sea level variation used in the model simulations and the timing of CM events (Table 2) are indicated, respectively, by the grey curve and the vertical shading (Figure 6). See the legend of Figure 7 for the definition of the different simulations.
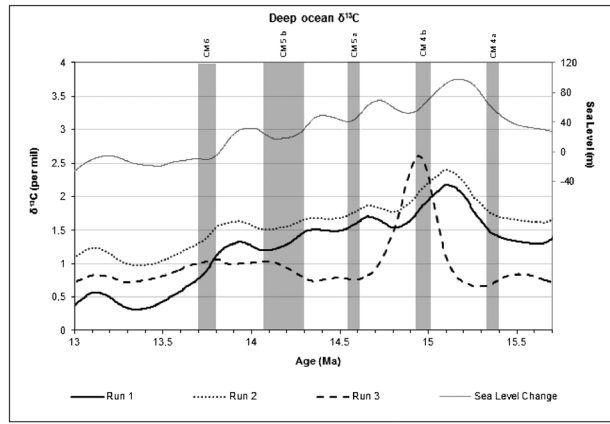
(see the supporting information). Short-term fluctuations in deep ocean $\delta^{13}C$ values are superimposed on this long-term trend and arise from the 400 kyr eccentricity cycle via the sea level boundary condition (Figure 8, solid line). Modeled maxima of $\delta^{13}C$ are out of phase with respect to the sea level forcing and tend to occur during sea level drops, just slightly earlier than sea level minima. The increases in modeled $\delta^{13}C$ are due to the deposition of organic carbon during sea level highstands, when the shelf area is larger. Maximum $\delta^{13}C$ is attained 70–80 kyr after the sea level maxima, due to the long turnover time of carbon in the ocean (100–200 kyr, obtained as the ratio between the reservoir size and total input or output flux), sourced by weathering fluxes, and drained by the deposition of carbon. As a result, the $\delta^{13}C$ maximum of the ocean occurs at the beginning of the cold period, just slightly before the minimum sea level is reached. This result is relatively consistent with the data, where CM events (maxima of $\delta^{13}C$) occur during cold periods (maxima of $\delta^{18}O$), at least within the temporal resolution of the data (~60 kyr).

[35] Driven by the external factor sea level, our results indicate that there is no direct link between enhanced oceanic productivity and eccentricity-induced global cooling on the one hand and $\delta^{13}C$ maxima during CM events on the other hand. The approximate temporal coincidence is due to internal lags in the carbon cycle of the ocean.

[36] While we now have an explanation for the timing of CM events, we note that the amplitudes of the modeled short-term $\delta^{13}C$ fluctuations (0.1–0.7‰, depending on the CM event considered; Figure 8) are significantly smaller than those of the records (amplitudes of 0.3–1.0‰, depending on the CM event and location considered; Figures 2–4). Can the modeled variations in $\delta^{13}C$ be amplified, for example, by changing the radiation balance and global temperature?

5.2. Albedo Forcing (Run 2)

[37] To analyze the possible impact of climate fluctuations on the model productivity and $\delta^{13}C$, the model was forced with the sea level variation as in the previous simulation, and in addition with an artificially enhanced albedo of the high latitudes during sea level lowstands, so as to force the model to produce global temperature variation locked to the sea level change. With this albedo forcing, the model produces a globally averaged warming of approximately 1.0 to 1.5°C when moving from low to high sea level conditions. In response to this simple glacial/interglacial cycle, silicate and carbonate weathering can be expected to vary, so that the input of phosphorus to the ocean—proportional to silicate weathering—varies in concert. But as shown in Figure 7 (run 2, dotted line), productivity is not much affected by this change and again does not show any significant variation associated with the 400 kyr cyclicity of sea level. Regarding the modeled $\delta^{13}C$ record, an overall shift of the curve toward slightly higher values is observed compared to the run without albedo forcing. The timing of the CM events is not significantly affected by this change (Figure 8, dotted line), but their amplitude is reduced.

5.3. Sensitivity to Ocean Circulation (Run 3)

[38] In a third sensitivity test, we prescribe changes in oceanic circulation. All model water fluxes between ocean reservoirs are multiplied by a factor (α) linearly related to sea level and assumed to be lower than 1 during sea level highstands (mimicking more sluggish ocean circulation during warm periods) and higher than 1 during sea level lowstands (mimicking more active circulation during cold periods). In addition to these fluctuations with a 400 kyr period and imposed by insolation and sea level, the intensity of ocean circulation also steadily increases between 15.2 and 12.7 Ma as a result of the overall long-term ice buildup, decrease in global sea level, and associated cooling. The imposed long-term downward trend in sea level and the associated invigorated circulation produce a strong long-term increase in productivity in the model experiment (Figure 7). As already discussed by *Diester-Haass et al.* [2009], such a global trend is not clearly supported by data.

[39] Importantly, however, with such a forcing of ocean circulation, it is possible to produce 400 kyr cycles in ocean productivity that have amplitudes comparable to observations (Figure 7, dashed line). Productivity is consistently higher during sea level lowstands, when circulation is more active and when more nutrients are mixed into the surface ocean from deep waters. Particularly striking is the modeled productivity response during CM 6 (~13.7 Ma; Figure 7). As a direct response to the sea level forcing, the model reproduces a double-peak productivity maximum during CM 6, with the first peak occurring near 13.8 Ma and the second one near 13.4 Ma (Figure 7), in excellent agreement with the timing of the double peak in productivity recorded by the BFAR data from Site 747 in the Southern Ocean (e.g., Figures 2 and 4, respectively).

[40] These changes in productivity can be expected to impact the ^{13}C isotopic composition of the ocean. As prescribed in the model, export productivity increases should be accompanied by an enhanced deposition of organic carbon in sediments and, hence, an increase in ocean $\delta^{13}C$ values. Because such changes in organic carbon deposition cannot change instantly the isotopic composition of the whole ocean due to the long turnover time (100–200 kyr) with respect to long-term carbon cycle, the $\delta^{13}C$ maximum should occur about 100 kyr after the productivity maximum.

Thus, maxima of organic carbon deposition associated with changes in the shelf area occurring during sea level highstands are recorded in the geologic record closer in time to, but before, the sea level lowstands, while those associated with productivity changes via ocean circulation should occur after sea level lowstands. The superposition of these two processes tends to dampen the fluctuations in the model $\delta^{13}C$ record. For example, model $\delta^{13}C$ maxima corresponding to CM 5a (~14.6 Ma) and CM 5b (14.3 Ma) have vanished (Figure 8). This is, however, not true for CM 4b (near 15 Ma), where the $\delta^{13}C$ maximum appears to be reinforced and shifted in time toward the cold phase (sea level lowstand), because the effect of circulation tends to exceed that of shelf area and weathering for this CM event (more than threefold increase in productivity between 15.2 and 14.9 Ma in response to circulation change). This pronounced maximum occurs at 14.95 Ma, in excellent agreement with the age of CM 4b in the data (Table 2). The CM 6 $\delta^{13}C$ maximum is visible in run 3, although its amplitude is very small. It occurs significantly later than in run 1 and is correctly placed (near 13.8 Ma) compared to CM 6 in the data. It is also shorter in duration than the maximum in ocean productivity (made of two peaks as discussed earlier; Figure 7, run 3) at the same period. This feature is also consistent with the data. Finally, it must be noted that in run 3, the long-term decreasing trend in $\delta^{13}C$ between 15 and 13 Ma has been removed, which is not consistent with the data.

[41] Consequently, the net effect on $\delta^{13}C$ values may critically depend on the exact balance between the effects of circulation and those of shelf area and weathering. Any discrepancy between the model and the data is strongly dependent on the (arbitrary) amplitude chosen for the circulation fluctuation, as well as on the magnitude of the organic fluxes (kerogen weathering and organic carbon burial) in the long-term carbon cycle, on which large uncertainties exist.

6. Discussion

[42] In sum, the geochemical model provides insights into the complex nature of the $\delta^{13}C$ and productivity relationships at the scale of individual CM events. The lack of a distinct, basin-wide signal in the productivity records even during CM 6 may reflect that it is difficult to pinpoint potential forcing factors. These results are in contrast to the Eocene-Oligocene and Oligocene-Miocene boundary, where both the geochemical models and BFARs support links between the $\delta^{13}C$ record, productivity, and carbon burial [*Zachos and Kump*, 2005; *Diester-Haass and Zahn*, 1996; *Pälike et al.*, 2006; *Diester-Haass et al.*, 2011; *Coxall and Wilson*, 2011]. The difference between these $\delta^{13}C$ maxima and CM 6 (and other CM events) may simply be their larger magnitude. Perhaps the changes in the external factors were not large enough to produce a distinct response above background variations.

[43] Periodic forcing via sea level and weathering cannot explain the productivity variations, but produces $\delta^{13}C$ variations of the correct temporal spacing, albeit not the correct amplitude. Because of the turnover time of carbon in the ocean with respect to external inputs of carbon, the $\delta^{13}C$ maxima, which reflect the enhanced storage of organic carbon on shelves during sea level highstands, occur later in the cycle and thus almost in association with sea level lowstands. Climate effects modeled via albedo feedbacks do not produce any significant changes in the modeled response in export productivity and the marine $\delta^{13}C$ record. Ocean circulation changes produce a response in export productivity that is in best agreement with the proxy records from Southern Ocean Site 747, in both the occurrence of regularly spaced maxima and in finer features such as the double productivity maximum during CM 6. The modeled $\delta^{13}C$ response is muted (except for CM 4b), however, which we ascribe to the fact that the oceanic carbon isotope budget is linked to two factors, a lagged response to external forcing (e.g., sea level/weathering) and a more immediate response to internal forcing (enhanced ocean circulation). Compared to the study of *Pälike et al.* [2006], the lower sensitivity of the model in terms of the $\delta^{13}C$ variation and its links to productivity possibly results from the integration of an oxygen cycle and associated negative feedbacks (e.g., an increase of circulation not only tends to increase productivity but also ventilates the thermocline, leading to a more efficient recycling of organic matter, hence limiting the increase of the organic carbon deposition flux).

[44] Model-data mismatches such as those evident in the underestimate of the $\delta^{13}C$ amplitude produced in run 1 may provide information regarding the nature of other unidentified feedbacks in the carbon cycle. For example, the model does not incorporate a sediment reservoir on the shelf. Such a sedimentary reservoir may help amplify the $\delta^{13}C$ fluctuations, since the organic carbon deposited on the shelf during sea level highstand may be weathered and released to the ocean at periods of low sea level, amplifying the difference between maxima and minima in the $\delta^{13}C$ record. Similar feedbacks may also be involved in the sediment layer within the thermocline or deep ocean reservoirs. The amount of organic carbon that is actually buried is a relatively small fraction of the organic carbon flux reaching the seafloor. In the model this fraction is constant in the absence of a sediment model, but in reality it may have varied significantly, which might have resulted into larger fluctuations of ocean $\delta^{13}C$. Another possibility is that increased organic deposition occurring on the shelf during sea level highstand is not only from marine origin, as assumed in the model, but also from continental origin (i.e., continental productivity would also exhibit eccentricity-driven variations).

[45] Model-data agreement exists in the eccentricity-scale export productivity variations produced and the occurrence of established CM events when ocean circulation is taken into consideration. As we have shown above, the BFAR productivity data, however, only show some correspondence between $\delta^{13}C$ and export productivity at Site 747. This is likely due to the fact that changes in ocean current velocities are a regional signal and do not vary homogeneously over the whole ocean as assumed for the sake of simplicity in the model. For example, shifts in upwelling zones may have occurred between the cold and warm phases of the eccentricity cycle. Also, the relationship between the change in sea level (or climate) and the change in ocean circulation is presumably not linear. However, the fact remains that the model is able, despite its simplicity, to reproduce the change in productivity as observed at least one site, Site 747 in the Southern Ocean.

[46] The relatively large productivity response at Site 747 found in the BFAR data reported here is consistent with increases in productivity inferred from planktic foraminiferal assemblage [*Verducci et al.*, 2009] at this site. However, changes in planktic foraminiferal assemblages can also be due to cooling, increased upper water column stratification, or salinity variations [*Majewski and Bohaty*, 2010]. In any case, the location of the site may be crucial. Enhanced paleoproductivity variations may reflect the location of the site in an area sensitive to climate-induced changes in the hydrographic regime. The distinct increase in export productivity during the cooler intervals at Site 747 points to the importance of the high latitudes as possible drivers of the pCO$_2$ decrease observed during the middle Miocene since 15 Ma [e.g., *van de Wal et al.*, 2011; *Badger et al.*, 2013] and should be tested at other high-latitude locations.

[47] The observed fluctuations of ocean productivity can only be replicated in the model by changes in ocean circulation, while changes in δ^{13}C are mainly associated (except for CM 4b) with the shelf area/weathering contribution to the deep ocean δ^{13}C fluctuations at eccentricity timescales. They tend to dampen the isotopic fluctuations associated with productivity changes directly (e.g., via ocean circulation) and may also induce temporal shifts of the δ^{13}C maxima.

[48] Hence, except for CM 4b, δ^{13}C fluctuations look to be dominated by shelf area and weathering variations, and maxima echo the previous sea level highstand with its increase of organic deposition associated with submerged shelf. Productivity, on the other hand, is kindled by more vigorous circulation and upper ocean mixing during cold periods marked by δ^{18}O maxima. As a result, the apparent positive relationship (or correlation) between δ^{13}C maxima and δ^{18}O maxima may be accidental.

7. Conclusions

[49] Middle Miocene paleoproductivity reconstructions were generated from BFARs to test the idea that pronounced benthic foraminiferal δ^{13}C variations in globally distributed sediment cores (the CM events of *Vincent and Berger* [1985]) can be related to changes in the marine carbon cycle [e.g., *Holbourn et al.*, 2007]. We find that one of the distinct positive excursions in δ^{13}C, the CM 6 event at 13.8 Ma, is consistently associated with maxima in paleoproductivity at Hole 588 and Site 747. Only at Site 747 are other CM events accompanied by paleoproductivity increases. Model results shed light on the ambiguous geochemical results: The δ^{13}C record of the deep ocean carbon reservoirs lags insolation by 70–80 kyr, and maxima may reflect enhanced carbon burial on expanded shelf areas during the previous sea level highstand. Productivity, on the other hand, is kindled by more vigorous circulation and upper ocean mixing during cold periods, especially during CM 6, as marked by δ^{18}O maxima, with lesser time lags. We conclude that the δ^{13}C output is muted likely due to the competing effects of the lagged response due to sea level and weathering changes versus productivity-driven variations linked to climate-induced changes in ocean circulation. However, the model was shown to underestimate the amplitude of the deep ocean δ^{13}C signal and to be slightly in advance of phase with respect to the data. The low sensitivity of the model may be linked to negative feedbacks associated with the oxygen cycle. Additional feedbacks not included in the model and involving oceanic sediments may amplify and/or delay the δ^{13}C response. Alternatively, the burial of land-derived organic carbon may also respond to the eccentricity cycle and have contributed to the δ^{13}C fluctuations. These hypotheses should be the focus of future research.

[50] A different picture emerges from Southern Ocean Site 747. Data here show distinct productivity maxima concurrent with δ^{18}O and δ^{13}C maxima throughout most of the middle Miocene, consistent with surface hydrographic variations perhaps due to the proximity to the Polar Frontal Zone. These results are consistent with the stipulation of *Holbourn et al.* [2007] who invoked eccentricity-scale high-latitude insolation changes as the primary driver of δ^{13}C variability via its effects in productivity and carbon burial.

References

Antoine, D., J.-M. Andre, and A. Morel (1996), Oceanic primary production. 2. Estimation at global scale from satellite (coastal zone color scanner) chlorophyll, *Global Biogeochem. Cycles*, *10*, 57–69.

Badger, M. S. P., C. H. Lear, R. D. Pancost, G. L. Foster, T. R. Bailey, M. J. Leng, and H. A. Abels (2013), CO2 drawdown following the middle Miocene expansion of the Antarctic Ice Sheet, *Paleoceanography*, *28*, 42–53, doi:10.1002/palo.20015.

Berger, W. H., and G. Wefer (1990), Export production: Seasonality and intermittency, paleoceanographic implications, *Palaeogeogr. Palaeoclimatol. Palaeoecol.*, *89*, 245–254.

Coxall, H. K., and P. A. Wilson, (2011), Early Oligocene glaciation and productivity in the eastern equatorial Pacific: Insights into global carbon cycling, *Paleoceanography*, *26*, PA2221, doi:10.1029/2010PA002021.

Dessert C., B. Dupré, L. M. François, J. Schott, J. Gaillardet, G. J. Chakrapani, and S. Bajpai (2001), Erosion of deccan traps determined by river geochemistry: Impact on the global climate and the ^{87}Sr/^{86}Sr ratio of seawater, *Earth Planet. Sci. Lett.*, *188*, 459–474.

Dessert C., B. Dupré, J. Gaillardet, L. M. François, and C. J. Allègre (2003), Basalt weathering laws and the impact of basalt weathering on the global carbon cycle, *Chem. Geol.*, *202*, 257–273.

Diester-Haass, L., and S. Nees (2004), Late Neogene history of paleoproductivity and ice rafting south of Tasmania, in *The Cenozoic Southern Ocean: Tectonics, Sedimentation, and Climate Change Between Australia and Antarctica*, *Geophys. Monogr. Ser.*, vol. 151, edited by N. F. Exon, J. P. Kennett, and M. J. Malone, pp. 253–272, AGU, Washington, D. C., doi:10.1029/148GM18.253-272.

Diester-Haass, L., and R. Zahn (1996), Eocene-Oligocene transition in the Southern Ocean: History of water mass circulation and biological productivity, *Geology*, *24*, 163–166.

Diester-Haass, L., P. A. Meyers, and T. Bickert (2004), Carbonate crash and biogenic bloom in the late Miocene: Evidence from ODP Sites 1085, 1086 and 1087 in the Cape Basin, southeast Atlantic Ocean, *Paleoceanography*, *19*, PA1007, doi:10.1029/2003PA000933.

Diester-Haass, L., K. Billups, and K.-C. Emeis (2005), In search of the late Miocene-early Pliocene "Biogenic Bloom" in the Atlantic Ocean (ODP Sites 982, 925, and 1088), *Paleoceanography*, *20*, PA4001, doi:10.1029/2005PA001139.

Diester-Haass, L., K. Billups, and K.-C. Emeis (2006), Late Miocene carbon isotope records and marine biological productivity: Was there a (dusty) link?, *Paleoceanography*, *21*, PA4216, doi:10.1029/2006PA001267,

Diester-Haass, L., K. Billups, D. R. Gröcke, L. François, V. Lefebvre, and K. C. Emeis (2009), Mid Miocene paleoproductivity in the Atlantic Ocean and implications for the global carbon cycle, *Paleoceanography*, *24*, PA1209, doi:10.1029/2008PA001605.

Diester-Haass, L., K. Billups, and K. C. Emeis (2011), Marine biological productivity and carbon cycling during the Oligocene to Miocene climate transition, *Palaeogeogr. Palaeoclimatol. Palaeoecol.*, *302*, 464–473.

Elmstrom, K. M., and J. P. Kennett (1986), Late Neogene paleoceanographic evolution of Site 590: Southwest Pacific, in *Initial Rep. Deep Sea Drill. Proj.*, *90*, 1361–1381.

Ennyu A., and M. A. Arthur (2004), Early to Middle Miocene paleoceanography in the southern high latitudes off Tasmania, in *The Cenozoic Southern Ocean: Tectonics, Sedimentation, and Climate Change Between Australia and Antarctica*, *Geophys. Monogr. Ser.*, vol. 151, edited by N. F. Exon, J. P. Kennett, M. J. Malone, pp. 215–233, AGU, Washington, D. C.

Flower, B. P., and J. P. Kennett (1993), Middle Miocene ocean-climate transition: High resolution oxygen and carbon isotopic records from Deep Sea Drilling Project Site 588A, southwest Pacific, *Paleoceanography*, *8*, 811–843.

Flower, B. P., and J. P. Kennett (1994), The middle Miocene climatic transition: East Antarctic ice sheet development, deep ocean circulation and global carbon cycling, *Palaeogeogr. Palaeoclimatol. Palaeoecol.*, *108*, 537–555.

Föllmi, K. B., C. Badertscher, E. de Kaenel, P. Stille, C. M. John, T. Adatte, and P. Steinmann (2005), Phosphogenesis and organic-carbon preservation in the Miocene Monterey Formation at Naples Beach, California: The Monterey hypothesis revisited, *Geol. Soc. Am. Bull.*, *117*, 589–619.

François L. M., and J. C. G. Walker (1992), Modelling the Phanerozoic carbon cycle and climate: Constraints from the ^{87}Sr/^{86}Sr isotopic ratio of seawater, *Am. J. Sci.*, *292*, 81–135.

Gaillardet J., B. Dupré, P. Louvat, and C. J. Allègre (1999), Global silicate weathering and CO_2 consumption rates deduced from the chemistry of the large rivers, *Chem. Geol.*, *159*, 3–30.

Herguera, J. C. (2000), Last glacial paleoproductivity patterns in the eastern equatorial Pacific: Benthic foraminifera records, *Mar. Micropal.*, *40*, 259–275.

Herguera, J. C., and W. A. Berger (1991), Paleoproductivity from benthic foraminifera abundance: Glacial to postglacial change in the west-equatorial Pacific, *Geology*, *19*, 1173–1176.

Hill, P. J., and N. F. Exon (2004), Tectonics and basin development of the offshore Tasmanian area incorporating results from deep ocean drilling, in *The Cenozoic Southern Ocean: Tectonics, Sedimentation, and Climate Change Between Australia and Antarctica*, *Geophys. Monogr. Ser.*, vol. 151, edited by N. F. Exon, J. P. Kennett, M. J. Malone, pp. 19–42, American Geophysical Union (AGU), Washington, D. C.

Holbourn, A., W. Kuhnt, M. Schulz, and H. Erlenkeuser (2005), Impacts of orbital forcing and atmospheric carbon dioxide on Miocene ice-sheet expansion, *Nature*, *438*, 483–487.

Holbourn, A., W. Kuhnt, M. Schulz, J.-A. Flores, and N. Andersen (2007), Orbitally paced climate evolution during the middle Miocene "Monterey" carbon-isotope excursion, *Earth Planet. Sci. Lett.*, *261*, 534–550.

Holdgate, G. R., I. Cartwright, D. T. Blackburn, M. W. Wallace, S. J. Gallagher, B. E. Wagstaff, and L. Chung (2007), The Middle Miocene Yallourn coal seam—The last coal in Australia, *Int. J. Coal Geol.*, *70*, 95–115.

Isaacs, C. M. (2001), Depositional framework of the Monterey formation, California, in *The Monterey Formation, From Rocks to Molecules*, edited by C. M. Isaacs and K. Rullkötter, pp. 1–30, Columbia Univ. Press, New York.

Kennett, J. P., and C. C. von der Borch (1986), Southwest Pacific Cenozoic paleoceanography, Deep Sea Drilling Project Leg 90, in *Initial Rep. Deep Sea Drill. Proj.*, *90*, Washington, 1493–1517.

Kump, L. R., and M. A. Arthur (1999), Interpreting carbon-isotope excursions: Carbonates and organic matter, *Chem. Geol. 161*, 181–198.

Lawver, L. A., L. M. Gahagan, and M.-F. Coffin (1992), The development of paleoseaways around Antarctica, in *The Antarctic Paleoenvironment: A Perspective on Global Change, Part One*, *Antarct. Res. Ser.*, vol. 56, edited by J. P. Kennett and D. A. Warnke, pp. 7–30, AGU, Washington, D. C.

Lefebvre, V. (2009), Modélisation numérique du cycle du carbone et des cycles biogéochimiques: Application aux perturbations climatiques de l'Ordovicien terminal, du Dévonien terminal et du Miocène moyen, PhD thesis, Univ. Lille 1, Villeneuve d'Ascq, France [Available at: http://ori-nuxeo.univ-lille1.fr/nuxeo/site/esupversions/c14d0084-96dd-49ca-9111-955897ff342c]

Lefebvre, V., T. Servais, L. François, and O. Averbuch (2010), Did a Katian Large Igneous Province trigger the Late Ordovician glaciation? A hypothesis tested with a carbon cycle model, *Palaeogeogr. Palaeoclimatol. Palaeoecol.*, *296*, 310–319.

Levitus, S., and T. P. Boyer (1994), World Ocean Atlas 1994, vol. 4, Temperature, NOAA Atlas NESDIS, vol. 4, 129 pp., NOAA, Silver Spring, Md.

Lourens, L., F. Hilgen, N. J. Shackleton, J. Laskar, and D. Wilson (2004), The Neogene period, in *A Geologic Time Scale*, F. Gradstein, J. Ogg, and A. Smith, pp. 409–440, Cambridge Univ. Press, Cambridge, U. K.

Mackensen, A., and W. U. Ehrmann (1992), Middle Eocene through Oligocene climate history and paleoceanography in the Southern Ocean: Stable oxygen and carbon isotopes from ODP Sites on Maud Rise and Kerguelen Plateau, *Mar. Geol.*, *108*, 1–27.

Majewski, W., and S. Bohaty (2010), Surface-water cooling and salinity decrease during the Middle Miocene Climate Transition at Southern Ocean ODP Site 747 (Kerguelen Plateau), *Mar. Micropaleontol.*, *74*, 1–14.

Millot R., J. Gaillardet, B. Dupré, and C. J. Allègre (2002), The global control of silicate weathering rates and the coupling with physical erosion: New insights from rivers of the Canadian Shield, *Earth Planet. Sci. Lett.*, *196*, 83–98.

Nees, S. (1997), Late Quaternary palaeoceanography of the Tasman Sea: The benthic foraminiferal view, *Palaeogeogr. Palaeoclimatol. Palaeoecol.*, *131*, 365–389.

Nelson, C. S., and P. J. Cooke (2001), History of oceanic front development in the New Zealand sector of the Southern Ocean during the Cenozoic—A synthesis, *N. Z. J. Geol. Geophys.*, *44*, 535–553.

Pälike, H., et al. (2006), The heartbeat of the Oligocene climate system, *Science*, *314*, 1894–1898.

Schlich, R., et al. (1989), Introduction, *Proc. Ocean Drill. Program Initial Rep., 120*, 7–23.

Schmiedl, G., and A. Mackensen (1997), Late Quaternary paleoproductivity and deep water circulation in the eastern South Atlantic Ocean: Evidence from benthic foraminifera, *Palaeogeogr. Palaeoclimatol. Palaeoecol.*, *130*, 43–80.

Shevenell, A. E., and J. P. Kennett (2007), Cenozoic Antarctic cryosphere evolution: Tales from deep-sea sedimentary records, *Deep Sea Res. II*, *54*, 2308–2324.

Shevenell, A. E., J. P. Kennett, and D. W. Lea (2008), Middle Miocene ice sheet dynamics, deep-sea temperatures, and carbon cycling: A Southern Ocean perspective, *Geochem. Geophys. Geosyst.*, *9*, Q02006, doi:10.1029/2007GC001736.

Shipboard Scientific Party (2001), Site 1171. In Exon, N. F., Kennett, J. P., Malone, M. J., et al., *Proc. ODP, Init. Proc. Ocean Drill. Program Initial Rep., 189*, 1–176, doi:10.2973/odp.proc.ir.189.106.2001.

Suess, E. (1980), Organic carbon flux in the oceans: Relation to surface productivity and oxygen utilization, *Nature*, *288*, 260–263.

Utescher, T., V. Mosbrugger, and A. Ashraff (2000), Terrestrial climate evolution in Northwest Germany over the last 25 million years, *Palaios*, *15*, 430–449.

Van Cappellen, P., and E. D. Ingall (1996), Redox stabilization of the atmosphere and oceans by phosphorus-limited marine productivity, *Science*, *271*, 493–496.

Van de Wal, R. S. W., B. de Boer, L. J. Lourens, P. Köhler, and R. Bintanja (2011), Reconstruction of a continuous high-resolution CO_2 record over the past 20 million years, *Clim. Past*, *7*, 1459–1469, doi:10.5194/cp-7-1459-2011.

Veizer, J., et al. (1999), ^{87}Sr/^{86}Sr, d^{13}C and d^{18}O evolution of Phanerozoic seawater, *Chem. Geol.*, *161*, 59–88.

Verducci, M., L. M. Foresi, G. H. Scott, M. Sprovieri, F. Lirer, and N. Pelosi (2009), The middle Miocene climatic transition in the Southern Ocean: Evidence of paleoclimatic and hydrographic changes at Kerguelen plateau from planktonic foraminifers and stable isotopes, *Palaeogeogr. Palaeoclimatol. Palaeocol.*, *280*, 371–386.

Vincent, E., and W. H. Berger (1985), Carbon dioxide and polar cooling in the Miocene: The Monterey hypothesis, in *The Carbon Cycle and Atmospheric CO2: Natural Variations Archean to Present*, *Geophys. Monogr. Ser.*, vol. 32, edited by E. T. Sundquist and W. S. Broecker, pp. 455–468, AGU, Washington, D. C., doi:10.1029/GM032p0455.

Waite, A., L. Diester-Haass, S. Gibbs, R. Rickaby, and K. Billups (2008), A top-down and bottom-up comparison of paleoproductivity proxies: Calcareous nannofossil Sr/Ca ratios and benthic foraminiferal accumulation rates, *Geochem. Geophys. Geosyst.*, *9*, Q06005, doi:10.1029/2007GC001812.

Walker, J. C. G., and J. F. Kasting (1992), Effects of fuel and forest conservation on future levels of atmospheric carbon dioxide, *Palaeogeogr. Palaeoclimatol. Palaeoecol.*, *97*, 151-189.

Woodruff, F., and S. M. Savin (1991), Mid-Miocene isotope stratigraphy in the deep sea: High resolution correlations, paleoclimatic cycles, and sediment preservation, *Paleoceanography*, *6*, 755–806.

Wright, J. D., and K. G. Miller (1992), Miocene stable isotope stratigraphy, Site 747, Kerguelen Plateau, *Proc. Ocean Drill. Program Sci. Results, 120*, 855–866.

Wright, J. G., K. G. Miller, and R. G. Fairbanks (1992), Early and middle Miocene stable isotopes: Implications for deepwater circulation and climate, *Paleoceanography*, *7*, 357–389.

Yasuda, H. (1997), Late Miocene-Holocene paleoceanography of the western equatorial Atlantic: Evidence from deep-sea benthic foraminifera, *Proc. Ocean Drill. Program Sci. Results*, *154*, 395–432.

Zachos, J. C., and L. R. Kump (2005), Carbon cycle feedbacks and the initiation of Antarctic glaciation in the earliest Oligocene, *Global Planet. Change*, *47*, 51–66.

Zachos, J., M. Pagani, L. Sloan, E. Thomas, and K. Billups (2001), Trends, rhythms, and aberrations in global climate 65 Ma to present, *Science*, *292*, 686–693.

van der Zwaan, G. J., I. A. P. Duijnstee, M. den Bulk, S. R. Ernst, N. T. Jannink, and T. J. Kouwenhoven (1999), Benthic foraminifers: Proxies or problems? A review of paleoecological concepts, *Earth Sci. Rev.*, *46*, 213–236.